

OPEN

Received: 17 February 2016 Accepted: 27 June 2016 Published: 22 July 2016

Hollow $Zn_xCd_{1-x}S$ nanospheres with enhanced photocatalytic activity under visible light

Ying Jin^{1,2,3}, Haoyun Zhang¹, Chuang Song², Lanfang Wang¹, Qingyi Lu¹ & Feng Gao²

Formation of solid solutions is a good strategy to acquire materials with special properties and bring forth new type of applications or enhance the performance of currently existing devices. In this study, hollow $Zn_xCd_{1-x}S$ nanospheres with different molar ratios were synthesized via a facile hydrothermal process. The products were fully characterized by X-ray diffraction, scanning electron microscopy, transmission electron microscopy, energy-dispersive X-ray spectroscopy, and UV-vis absorption spectroscopy. It was found that the photocatalysis performance of the as-prepared samples could be enhanced by formation of $Zn_xCd_{1-x}S$ solid solutions. In addition, their photocatalytic activities are dependent on the Zn/Cd molar ratios and nanostructures of $Zn_xCd_{1-x}S$ solid solutions. Hollow $Zn_{0.2}Cd_{0.8}S$ spheres exhibit extremely high photocatalytic activity and good re-usability, and the photocatalytic conversion of RhB reaches as high as 96% after 50 min of irradiation.

Over the past decades, growing attention regarding environmental and energy problems have stimulated wide researches on solar energy untilization. Among them, using semiconductor photocatalysts to degrade organic dyes are extensively explored^{1,2}. But most of semiconductor photocatalysts, such as TiO_2 and ZnO, can only absorb UV light for photocatalytic activation due to their wide band gaps^{3,4}. Since UV light accounts for a small portion (5%) of the solar spectrum as compared to visible light (52%)⁵, how to design high-performanced photocatalysts with suitable band gap for maximally utilizing visible light becomes important⁶.

II-VI semiconductor CdS with an appropriate band gap $(2.4\,\mathrm{eV})$ is regarded as an outstanding visible-light responsive material for photocatalysts^{7,8}. However, the low separation efficiency of photogenerated electrons (e⁻) and holes (h⁺) and the fact that it is easily corroded^{9,10}, limit its applications in solar conversion and environmental remediation. Enormous attention has been devoted to finding ways to overcome this weakness of CdS, such as coupling CdS with another semiconductor^{11,12}, embedding CdS particles in graphene or polymer matrix^{13,14}, and formation of solid solutions^{15,16}. Among these strategies, formation of solid solutions is considered to be a good strategy to acquire materials with many unique properties^{17,18}. $Zn_xCd_{1-x}S$, a kind of ternary transition metal sulfides has fine and tunable absorption in the visible region of solar energy and excellent electrical conductibility, which has been recognized as compatible candidates for photocatalysts^{19,20}. Various kinds of nanostructures of $Zn_xCd_{1-x}S$, such as quantum dots^{21,22}, nanoparticles²³, nanowires²⁴, nanobelts²⁵, nanorods²⁶, and nanoribbons²⁷ have been prepared, while the hollow structured $Zn_xCd_{1-x}S$ have not been reported so far. Hollow structured materials show many advantages including porous structure, large surface area, high light-harvesting efficiency and fast mobility of charge carriers, and have promising application in the field of photocatalytic processes. Therefore, the design and fabrication of $Zn_xCd_{1-x}S$ hollow structure is one admirable strategy in photocatalysis.

Herein, we propose a simple straightfoward route to prepare $Zn_xCd_{1-x}S$ hollow spheres with the assistance of carboxymethyl cellulose (CMC) under hydrothermal conditions. This one-step route provides both the expected hollow structure and ternary chalcorenide $Zn_xCd_{1-x}S$ semiconductors with different molar ratios. More importantly, the as-obtained hollow $Zn_xCd_{1-x}S$ spheres exhibit great enhancement of photocatalytic activities for the degradation of Rhodamine B (RhB) under visible-light irradiation.

¹State Key Laboratory of Coordination Chemistry, Coordination Chemistry Institute, Collaborative Innovation Center of Advanced Microstructures, Nanjing National Laboratory of Microstructures, School of Chemistry and Chemical Engineering, Nanjing University, Nanjing 210093, P. R. China. ²Department of Materials Science and Engineering, Collaborative Innovation Center of Advanced Microstructures, Nanjing National Laboratory of Microstructures, Nanjing University, Nanjing 210093, P. R. China. ³College of Biological and Chemical Engineering, Anhui Polytechnic University, Wuhu 241000, Anhui P. R. China. Correspondence and requests for materials should be addressed to Q.L. (email: qylu@nju.edu.cn) or F.G. (email: fqao@nju.edu.cn)

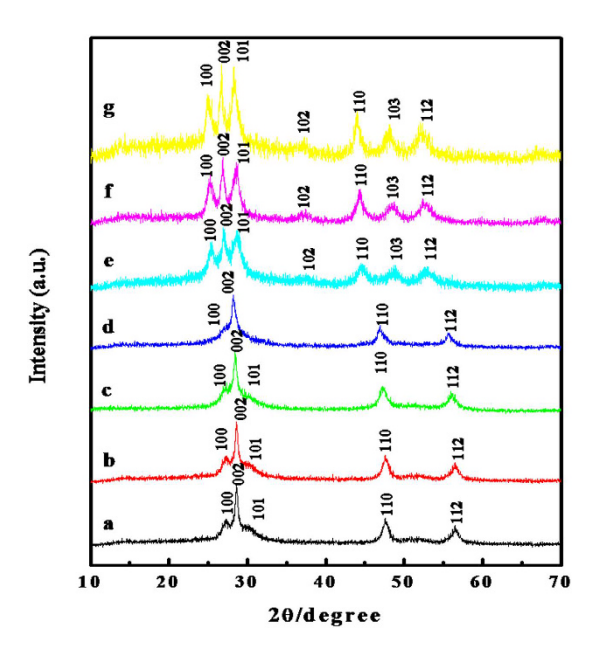


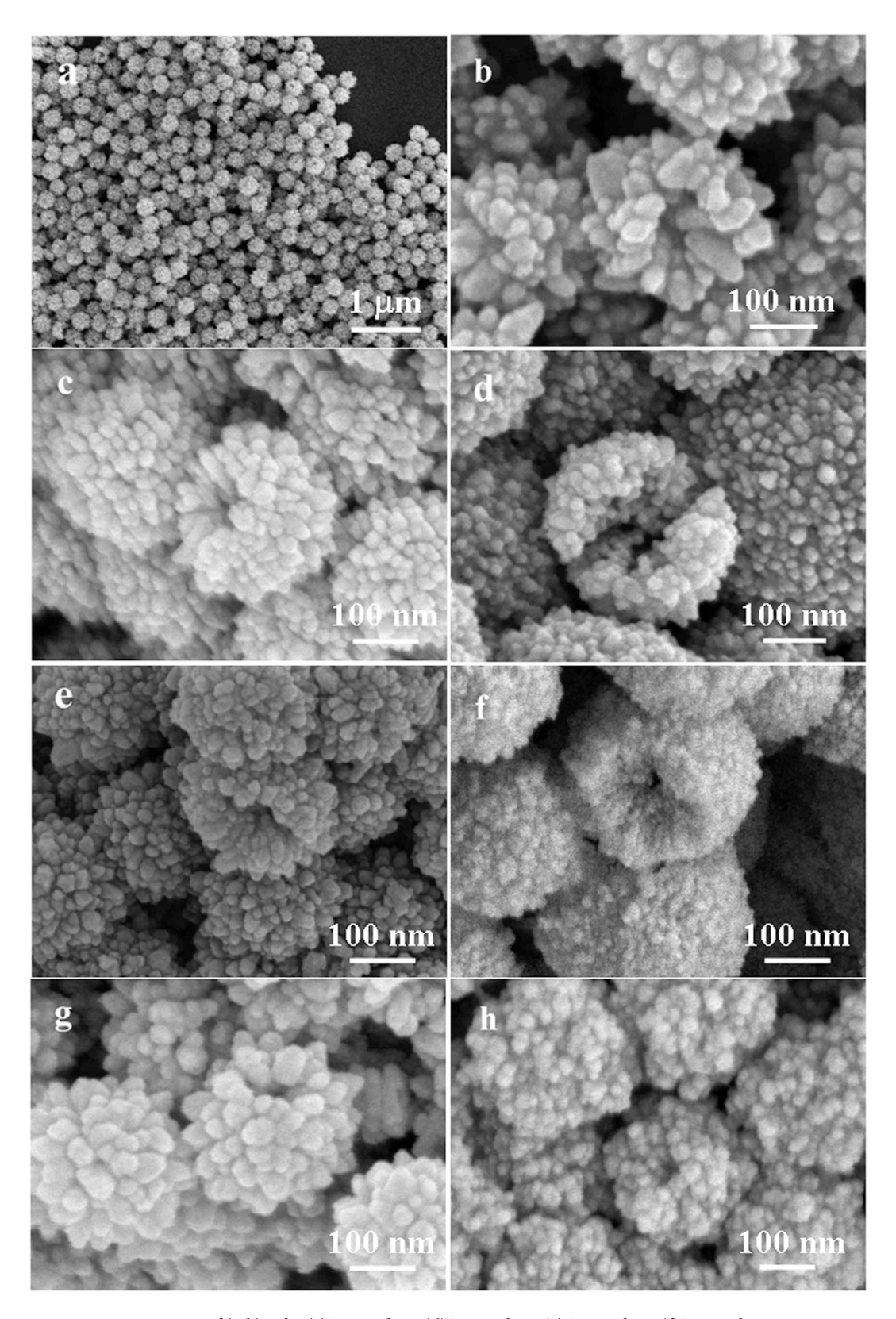
Figure 1. XRD patterns of $Zn_xCd_{1-x}S(0 \le x \le 1)$ samples (a) ZnS; (b) $Zn_{0.9}Cd_{0.1}S$; (c) $Zn_{0.8}Cd_{0.2}S$; (d) $Zn_{0.5}Cd_{0.5}S$; (e) $Zn_{0.2}Cd_{0.8}S$; (f) $Zn_{0.1}Cd_{0.9}S$; (g) $Zn_{0.1}Cd_{0.9}S$

Results and Discussion

A series of $Zn_xCd_{1-x}S$ hollow spheres were prepared with the assistance of carboxymethyl cellulose (CMC) and ammonia via a hydrothermal process, using zinc acetate, cadmium nitrate and l-cysteine as reactants. The molar ratios of Zn and Cd used were 10:0, 9:1, 8:2, 1:1, 2:8, 1:9 and 0:10, and the corresponding resulting products were labeled as ZnS, $Zn_{0.9}Cd_{0.1}S$, $Zn_{0.8}Cd_{0.2}S$, $Zn_{0.5}Cd_{0.5}S$, $Zn_{0.2}Cd_{0.8}S$, $Zn_{0.1}Cd_{0.9}S$, and CdS, respectively. Figure 1 shows X-ray diffraction (XRD) patterns of the as-prepared ZnS, $Zn_xCd_{1-x}S$ and CdS samples. The diffraction peaks observed at 27.0°, 28.5° and 30.6° in Fig. 1a can be indexed to (100), (002) and (101) of the hexagonal structure of ZnS (JCPDS, 01-0677), while the diffraction peaks at 24.8°, 26.4° and 28.1° in Fig. 1g can be indexed to (100), (002) and (101) of the hexagonal structure of CdS (JCPDS, 41-1049), respectively. In the case of $Zn_{0.9}Cd_{0.1}S$, $Zn_{0.8}Cd_{0.2}S$, $Zn_{0.5}Cd_{0.5}S$, $Zn_{0.2}Cd_{0.8}S$, $Zn_{0.1}Cd_{0.9}S$ products, from the XRD patterns in Fig. 1b-f, all the samples have a hexagonal crystal phase and all of the diffraction patterns are similar but with the obvious diffraction peak shifts. In a general way, since the ionic radius of Zn^{2+} is smaller than that of Zn^{2+} , the increasing of Zn/Zn molar ratios leads to the shrinkage of the unit-cell volume of the $Zn_xCd_{1-x}S$ samples. Therefore, all the diffraction peaks shift to the higher angles with increasing the Zn^{2+} concentration as shown in Fig. 1, which indicates that the $Zn_xCd_{1-x}S$ solid solutions have been successfully prepared.

The morphology of these $Zn_*Cd_{1-*}S$ samples was investigated by scanning electron microscopy (SEM). Figure 2a shows a typical SEM image of the obtained CdS sample, which clearly displays that the sample consists of uniform nanospheres with an average diameter of 300 nm. Some open pores in the image obviously suggest the hollow nature of the nanospheres. A magnified SEM image (Fig. 2b) shows that the shells of these hollow nanospheres are rough and consist of many small CdS nanoparticles. Figure 2c~h show the SEM images of Zn_{0.9}Cd_{0.1}S, $\bar{Z}n_{0.8}Cd_{0.2}S$, $Zn_{0.5}Cd_{0.5}S$, $Zn_{0.2}Cd_{0.8}S$, $Zn_{0.1}Cd_{0.9}S$ and $\bar{Z}nS$ samples. It can be clearly observed that similar to CdS sample, with the increase of Zn content in the solid solutions, the obtained samples are all hollow structures with diameters of about 300 nm and the shell of the hollow structures are composed of small nanoparticles. In the process of reaction, both ammonia and carboxymethyl cellulose (CMC) play key roles in the formation of the $Zn_xCd_{1-x}S$ hollow structures. It is known that CMC is a kind of water soluble polyanionic compounds with a large number of carboxyl and hydroxyl groups. With the addition of CMC in the reaction system, the solution could be divided into numerous homogeneous "chambers" 28, which can serve as soft templates to confine the growth of $Zn_xCd_{1-x}S$ during the growth process. Without the addition of CMC, only particles and irregular microspheres were obtained (Figure S1a,b). With the addition of CMC but in the absence of ammonia, uniform spheres can be achieved but these spheres are hard (Figure S1c,d). Even with the both addition of CMC and ammonia, if shorten the reaction time to one hour, only solid sphere products can be obtained (Figure S2). The "chambers" confine the crystal growth to form $Zn_xCd_{1-x}S$ nanoparticles and the assembly function of CMC further assembles these nanoparticles into uniform spheres. Ammonia can reacts with Zn^{2+} and Cd^{2+} to form $[Zn(NH_3)_4]^{2+}$ and $[Cd(NH_3)_4]^{2+}$ complexes, respectively. Under the hydrothermal conditions, after $Zn_xCd_{1-x}S$ spheres form, the existence of ammonia makes $Zn_xCd_{1-x}S$ dissolve to form $Zn[(NH_3)_4]^{2+}$ and $[Cd(NH_3)_4]^{2+}$ complexes. So, in the reaction system dissolution-precipitation dynamic equilibrium is presented:

$$Zn_{x}Cd_{1-x}S \,+\, 4NH_{3} \Leftrightarrow x[Zn(NH_{3})_{4}]^{2^{+}} \,+\, (1-x)\!\big[Cd(NH_{3})_{4}\big]^{2^{+}} \,+\, S^{2^{-}}$$



 $\begin{aligned} \textbf{Figure 2.} & \text{ SEM images of (a,b) CdS; (c) } Zn_{0.1}Cd_{0.9}S; \textbf{(d) } Zn_{0.2}Cd_{0.8}S; \textbf{(e) } Zn_{0.5}Cd_{0.5}S; \textbf{(f) } Zn_{0.8}Cd_{0.2}S; \textbf{(g) } Zn_{0.9}Cd_{0.1}S; \textbf{(h) } ZnS \text{ nanospheres.} \end{aligned}$

Under the dissolution-precipitation dynamic balance, based on the Ostwald's ripening process, smaller $Zn_xCd_{1-x}S$ particles dissolve and the surface nanoparticles grow bigger. With continuous dissolve of the core $Zn_xCd_{1-x}S$ small particles, inner cavities eventually form, resulting in the formation of $Zn_xCd_{1-x}S$ hollow nanospheres.

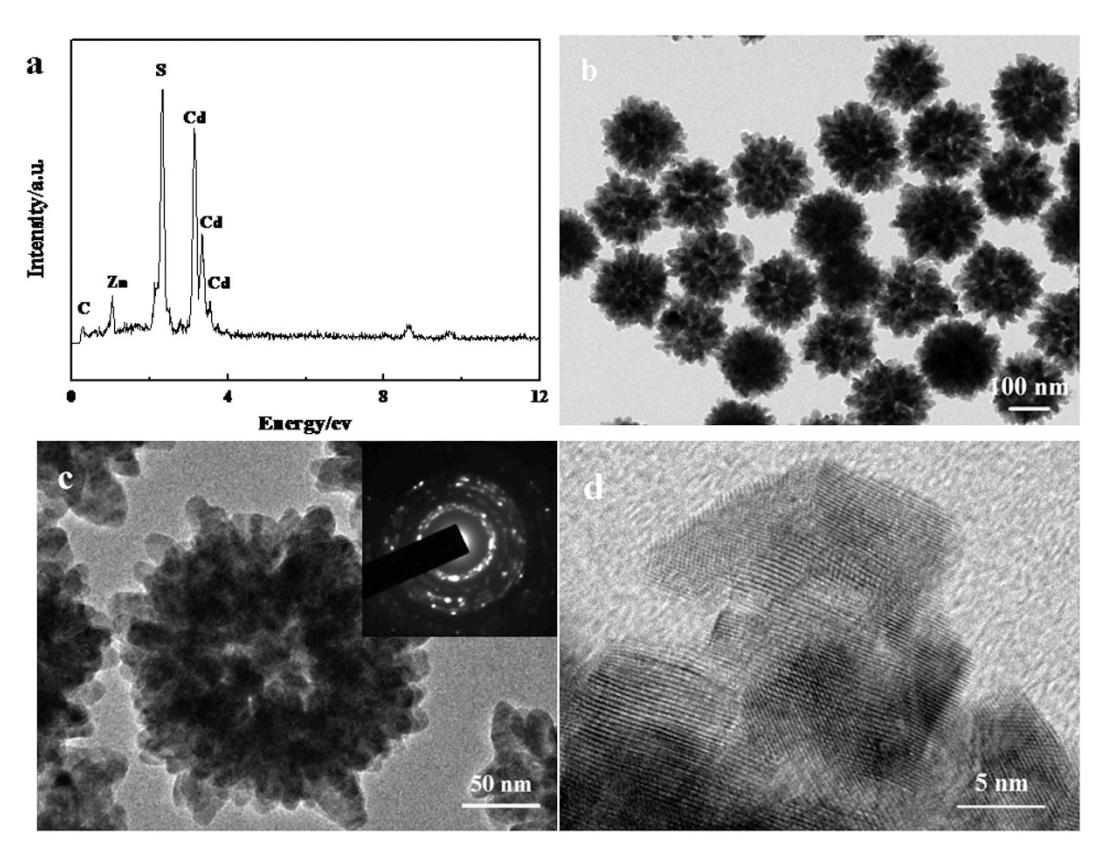


Figure 3. (a) EDS pattern; (b,c) TEM images and (d) HRTEM image of the as-prepared $Zn_{0.2}Cd_{0.8}S$ hollow spheres. Inset in (c) SAED pattern of the $Zn_{0.2}Cd_{0.8}S$ hollow sphere.

The composition, morphology and structure of the as-prepared $Zn_xCd_{1-x}S$ hollow spheres were further elucidated by energy dispersive X-ray spectroscopy (EDS) and transition electron microscopy (TEM). Figure 3 displays the EDS pattern, TEM and HRTEM images of the obtained $Zn_{0.2}Cd_{0.8}S$ nanospheres. From the EDS pattern in Fig. 3a, the coexistence of Zn, Cd and S elements in the sample can be easily demonstrated, and quantitative analysis confirmed that the atom ratio of Zn/Cd/S is about 1:4:5, which is consistent with the used molar ratio of the reactants. The hollow structure was further confirmed by TEM image, in which a sharp contrast between the center and the boundary of the spheres can be clearly observed (Fig. 3b). Furthermore, a single hollow sphere TEM image (Fig. 3c) also reveals the hollow structure of $Zn_{0.2}Cd_{0.8}S$ and the hollow spheres is composed of small nanoparticles. The selected area electron diffraction (SAED) pattern inset in Fig. 3c indicates the polycrystalline nature of the hollow $Zn_{0.2}Cd_{0.8}S$ spheres. Figure 3d displays a high-resolution TEM (HRTEM) image of $Zn_{0.2}Cd_{0.8}S$ sample, from which the lattice fringes are clearly visible and the spacing is about 0.338 nm, which corresponds to (002) lattice plane of hexagonal $Zn_{0.2}Cd_{0.8}S$.

The optical property measurement of Zn_xCd_{1-x}S hollow spheres and solid Zn_{0.2}Cd_{0.8}S sphere, using the UV-vis diffuse reflectance spectra (DRS), were shown in Fig. 4. DRS of $Zn_xCd_{1-x}S$ hollow spheres are shown in Fig. 4a. CdS hollow spheres shows a sharp absorption edge at around 560 nm, and the absorption edge for the Zn_xCd_{1-x}S solid solutions with the increase of x value shows a blue-shift in turn relative to those of the hollow CdS spheres in the visible-light region, which further confirms the formation of the solid solution and indicates that the hollow $Zn_xCd_{1-x}S$ spheres have a bigger band gap than the CdS hollow spheres. Moreover, there is an enhanced light absorbance in the visible light region for $Zn_{0.2}Cd_{0.8}S$ and $Zn_{0.1}Cd_{0.9}S$ hollow spheres than CdS sample, which means a small x value would be beneficial to improve the absorption of visible light for $Zn_xCd_{1-x}S$ solid solutions. Plots obtained through the Kubelka-Munk transformation from the UV-vis diffuse reflectance spectra of all the prepared nanostructures are shown in Figure S3, from which the roughly estimated band gap energy (Eg) values are 2.29, 2.36, 2.42, 2.44, 2.48 and 2.66 eV for CdS, $Zn_{0.1}Cd_{0.9}S$, $Zn_{0.2}Cd_{0.8}S$, $Zn_{0.5}Cd_{0.5}S$, $Zn_{0.8}Cd_{0.2}S$ and $Zn_{0.9}Cd_{0.1}S$, respectively. tively. In Fig. 4b, hollow and solid Zn_{0.2}Cd_{0.8}S spheres' DRS spectra were shown, which display that the absorption band edges are 534 and 520 nm for hollow and solid Zn_{0.2}Cd_{0.8}S sphere, respectively. The direct band-gap values of the hollow $Zn_{0.2}Cd_{0.8}S$ spheres and solid $Zn_{0.2}Cd_{0.8}S$ sphere can be estimated to be about 2.32 and 2.38 eV, respectively. tively. Moreover, the visible light absorption of the hollow $Zn_{0.2}Cd_{0.8}S$ spheres was clearly stronger than that of solid Zn_{0.2}Cd_{0.8}S spheres. The results show that both the Zn/Cd molar ratio and nanostructures of sample affect its optical properties and the formation of hollow solid solution would be beneficial to their photocatalytic performances.

In order to determine the potential applications of $Zn_xCd_{1-x}S$ hollow spheres, the photocatalytic performances of products were evaluated by the photodegradation of RhB, one of the common dyes, in aqueous solution under visible light. Figure 5a shows the absorption spectra of the dye solution in the presence of $Zn_{0.2}Cd_{0.8}S$ hollow spheres under exposure to visible light. At the beginning, RhB shows a major absorption band at 554 nm. With the irradiation time

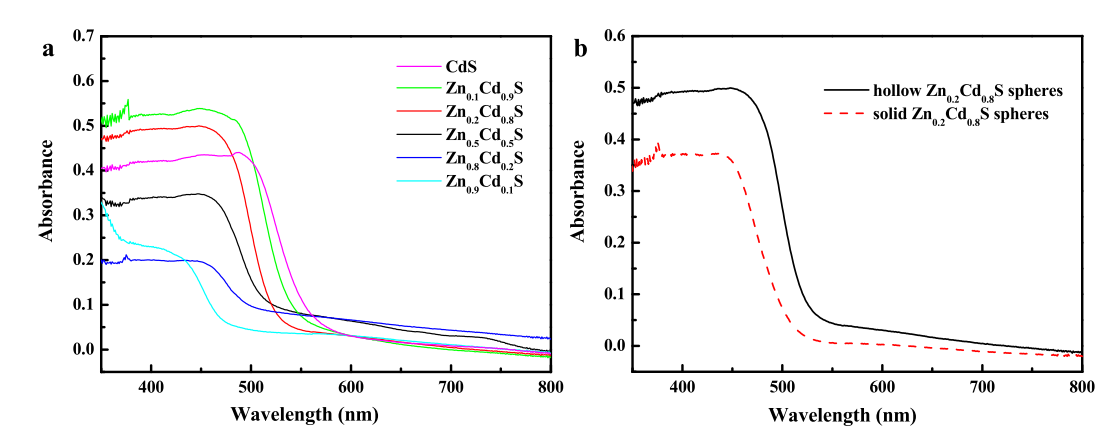


Figure 4. (a) UV-vis DRS of CdS and $Zn_xCd_{1-x}S$ ($0 \le x < 1$) samples; (b) UV-vis DRS of hollow $Zn_{0.2}Cd_{0.8}S$ spheres and solid $Zn_{0.2}Cd_{0.8}S$ spheres.

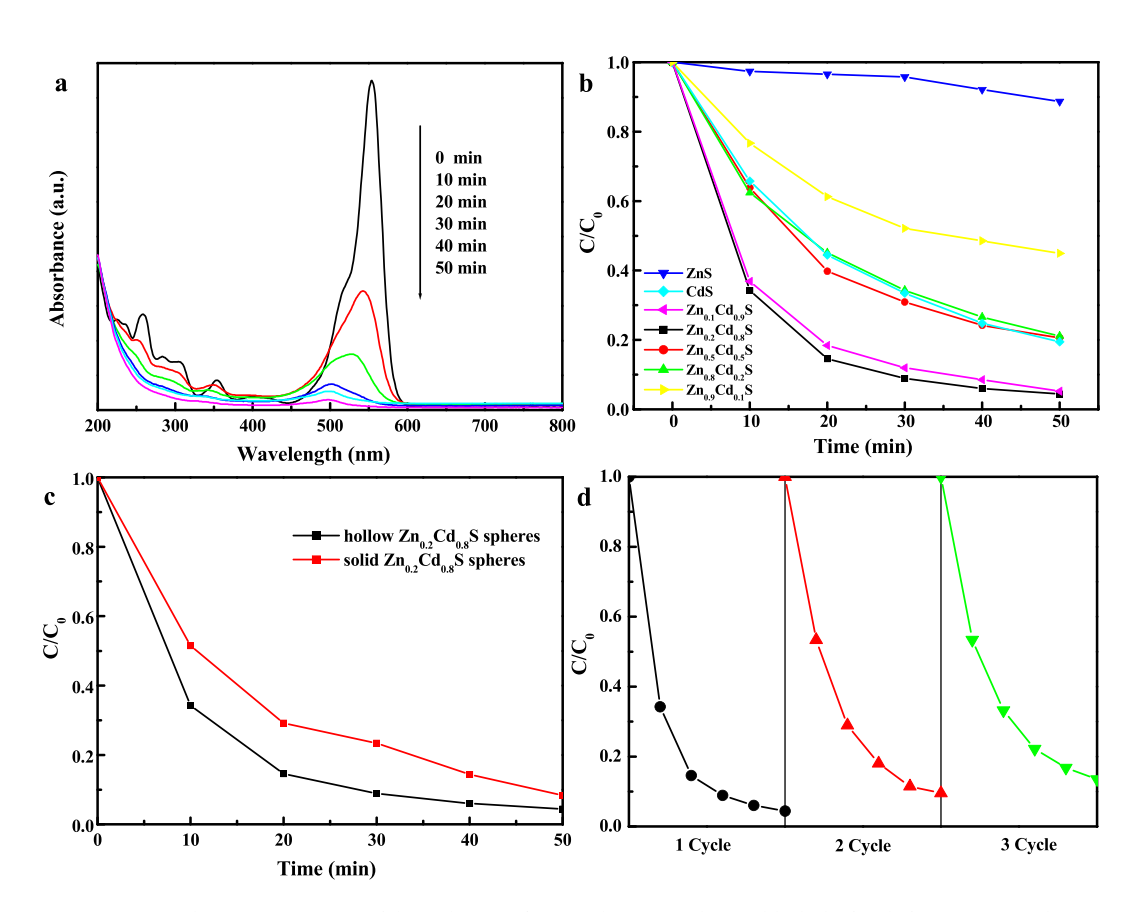


Figure 5. (a) Absorption spectra of dye solution after irradiation under visible-light for different time with the presence of $Zn_{0.2}Cd_{0.8}S$ hollow spheres; (b) C/C_0 versus time curves of dye solution under visible-light irradiation with different photocatalysts; (c) C/C_0 versus time curves of dye solution under visible-light irradiation with hollow $Zn_{0.2}Cd_{0.8}S$ spheres and solid $Zn_{0.2}Cd_{0.8}S$ spheres samples as photocatalysts; (d) Three cycles using hollow $Zn_{0.2}Cd_{0.8}S$ spheres photocatalyst under visible-light irradiation for 50 min.

prolonging, the absorption peak at $554\,\mathrm{nm}$ is blue-shift and decreases quickly. The shift of the absorption is caused by de-ethylation of RhB because of the attack by one of the active oxygen species on the N-ethyl group and RhB is transformed to rhodamine. Rhodamine can be then further decomposed due to the further destruction of the conjugated. During this process, the measured absorbance (A) would be the sum of the absorbances of remaining RhB and its decomposition product. After 50 min degradation, the absorbance of the dye solution decreases to 4% of the original absorbance, which means both RhB and rhodamine have been almost decomposed and indicates $\mathrm{Zn_{0.2}Cd_{0.8}S}$ hollow spheres exhibit high photocatalytic activities for the decomposition of RhB.

Figure 5b presents the dye residue concentration ratio (C/C_0 , calculated from A/A_0) with different samples as photocatalysts under different irradiation times. It can be clearly found that $Zn_{0.2}Cd_{0.8}S$ and $Zn_{0.1}Cd_{0.9}S$ hollow spheres show high photocatalytic activities compared to other samples, and the photocatalytic conversion of RhB with hollow $Zn_{0.2}Cd_{0.8}S$ spheres reaches as high as 96% after 50 min of irradiation. The degradation of RhB over the as-prepared catalysts with a 50 minute irradiation time decreased in the order of $Zn_{0.2}Cd_{0.8}S > Zn_{0.1}Cd_{0.9}S > Zn_{0.5}Cd_{0.5}S > Zn_{0.8}Cd_{0.2}S \approx CdS > Zn_{0.9}Cd_{0.1}S > ZnS$. Because of the large band gap of ZnS (3.7 eV), ZnS show relatively low photocatalytic activity under visible light. But what is worthy noting that most of hollow $Zn_xCd_{1-x}S$ spheres show enhanced activities than CdS hollow spheres, this result suggests that formation of $Zn_xCd_{1-x}S$ solid solutions can improve the photocativity of CdS. The Zn/Cd molar ratio has a great effect on the photocatalytic activity of $Zn_xCd_{1-x}S$ solid solutions and $Zn_{0.2}Cd_{0.8}S$ shows the best performances.

Not only Zn/Cd molar ratios of $Zn_xCd_{1-x}S$ samples affects the photocatalytic activities of the composite, but nanostructures of $Zn_xCd_{1-x}S$ also affect its photocatalytic performances. Figure 5c shows the curves of the dye residue concentration ratio as a function of irradiation time with different $Zn_{0.2}Cd_{0.8}S$ nanostructures. The photocatalytic activity of hollow $Zn_{0.2}Cd_{0.8}S$ sphere is clearly better than that of solid $Zn_{0.2}Cd_{0.8}S$ spheres as shown in Fig. 5c. This could be ascribed to the unique hollow structure of $Zn_{0.2}Cd_{0.8}S$ sample. The adsorption of contaminant molecules, light irradiation absorption, charge transportation and separation are three crucial factors for the photocatalytic activities of the composite²⁰. Firstly, the hollow $Zn_{0.2}Cd_{0.8}S$ sphere have much stronger visible light adsorbance and a smaller band gap according to UV-vis DRS (Fig. 4b). Secondly, the void interiors structure of $Zn_{0.2}Cd_{0.8}S$ hollow spheres provides both inner and outer surfaces to interact with RhB molecules, allowing multiple reflections of visible light within the interior cavities and benefiting electrons and holes transportation and separation²¹. The BET measurements of the hollow and solid $Zn_{0.2}Cd_{0.8}S$ spheres are provided in Figure S5. The BET surface area of the $Zn_{0.2}Cd_{0.8}S$ hollow spheres is calculated to be $Zn_{0.2}Cd_{0.8}S$ solid spheres ($Zn_{0.2}Cd_{0.8}S$ solid spheres ($Zn_{0.2}Cd_{0.8}S$ hollow spheres is calculated to be $Zn_{0.2}Cd_{0.8}S$ solid spheres ($Zn_{0.2}Cd_{0.8}S$ solid spheres ($Zn_{0.2}Cd_{0.8}S$ hollow spheres is calculated to be $Zn_{0.2}Cd_{0.8}S$ solid spheres ($Zn_{0.2}Cd_{0.8}S$ hollow spheres ($Zn_{0.2}Cd_{0.8}S$ solid spheres ($Zn_{0.2}Cd_{0.8}S$ hollow spheres spheres are provided in Figure S5.

Stability and re-usability is an important standard to measure a photocatalyst. So, we further investigated the durability of hollow $Zn_{0.2}Cd_{0.8}S$ sphere photocatalyst by collecting and reusing the photocatalyst for three cycles. Figure 5d shows the degradation percentage of dye solution maintained up to 90% even for the third cycle after 50 min photodegradation. The photocatalytic performance of the hollow $Zn_{0.2}Cd_{0.8}S$ sphere has a small loss due to the loss of catalyst during each cycle of collecting and cleaning. These results indicate that $Zn_{0.2}Cd_{0.8}S$ hollow sphere are photostable and reusable in the degradation of RhB.

Conclusions

We demonstrated in this work an effective hydrothermal route for the synthesis of solid solution $Zn_xCd_{1-x}S$ hollow spheres. The prepared $Zn_xCd_{1-x}S$ hollow spheres show the enhanced photocatalytic activity for the degradation of RhB under visible light ($\lambda > 420$ nm) irradiation, and hollow $Zn_{0.2}Cd_{0.8}S$ spheres were found to be highly efficient for RhB removal. Moreover, this hollow spherical $Zn_xCd_{1-x}S$ catalyst showed improved stability and would have great application potential in water treatment.

Methods

Synthesis of Zn_xCd_{1-x}S hollow microspheres. In a typical synthesis, the appropriate molar ratios of $Zn(CH_3COO)_2 \cdot 2H_2O$ and $Cd(NO_3)_2 \cdot 5H_2O$ with the sum mole number of Zn^{2+} and Cd^{2+} being 0.5 mmol were dissolved in a solution of sodium carboxymethyl cellulose (3 g/L in H_2O , 18 mL) with magnetic stirring, then ammonia (25%, analytically pure, 3 mL) and l-cysteine (analytically pure, 3 mmol) were added under magnetic stirring. After stirring for 10 min, the mixture was transferred into a 40 mL autoclave. The autoclave was sealed, heated at 150 °C for 6 h, and cooled down to room temperature naturally. The precipitate was collected by centrifugation, washed with distilled water and ethanol several times, and then dried at 60 °C for 12 h. The same procedures were applied to synthesize CdS hollow spheres and ZnS sample, respectively.

Characterizations. Powder X-ray diffraction (XRD) patterns were collected by using a Bruker D8 ADVANCE diffractometer with CuK_{α} radiation (λ = 1.5418 Å). The morphology of the samples were characterized by scanning electron microscopy (SEM, Hitachi S-4800). Energy-dispersive X-ray spectroscopy (EDS) attached to the SEM instrument was used to analyze the composition of the $Zn_xCd_{1-x}S$ samples. Transmission electron microscopy (TEM), high-resolution TEM (HRTEM) images, and the corresponding selected area electron diffraction (SAED) were obtained with a JEOL JEM-2100 instrument transmission electron microscope at an acceleration voltage of 200 KV. UV/Vis diffusion reflectance spectra (DRS) of the samples were studied with a UV-3600 spectrophotometer (Shimadzu, Japan) and BaSO₄ was used as the reference.

Photocatalytic Studies. The photocatalytic activities of the synthesized samples for the photocatalytic decolorization of an aqueous solution of Rhodamine B (RhB) were evaluated as follows: the as-prepared sample (20 mg) was suspended in a aqueous solution of RhB (1.0×10^{-5} M, 80 mL) in a beaker at ambient temperature. A 300 W xenon lamp was used as the visible-light source with a cutoff filter to cut off the light below 420 nm. Before irradiation, the suspension was continuously magnetically stirred in the dark for 60 min to achieve the adsorption–desorption equilibrium between the photocatalyst powder and the dye. Then, the photocatalytic reaction was initiated. At specific time intervals, 4 ml of the aqueous solution was taken and separated through centrifugation (10000 rpm) for the absorbance measurements, which were recorded with a Hitachi U-3900 spectrophotometer.

References

- 1. Chen, X. B., Liu, L. & Huang, F. Q. Black titanium dioxide (TiO₂) nanomaterials. Chem. Soc. Rev. 44, 1861–1885 (2015).
- 2. Liu, L. & Chen, Titanium dioxide nanomaterials: Self-structural modifications. X. Chem. Rev. 114, 9890–9918 (2014).

- Chen, X. B. & Mao, S. S. Titanium dioxide nanomaterials: Synthesis, properties, modifications, and applications. Chem. Rev. 107, 2891–2959 (2007).
- 4. Tian, C. G. et al. Cost-effective large-scale synthesis of ZnO photocatalyst with excellent performance for dye photodegradation. Chem. Commun. 48, 2858–2860 (2012).
- 5. Tan, L. L., Chai, S. P. & Mohamed, A. R. Synthesis and applications of graphene-based TiO₂ photocatalysts. *ChemSusChem* 5, 1868–1882 (2012).
- Zhang, N., Zhang, Y., Pan, X., Yang, M. & Xu, Y. Constructing ternary CdS-graphene-TiO₂ hybrids on the flatland of graphene oxide with enhanced visible-light photoactivity for selective transformation. J. Phys. Chem. C 116, 18023–18031 (2012).
- 7. Bera, R., Kundu, S. & Patra, A. 2D Hybrid nanostructure of reduced graphene oxide—CdS nanosheet for enhanced photocatalysis. *ACS Appl. Mater. Interfaces* 7, 13251–13259 (2015).
- 8. Zong, X. et al. Enhancement of photocatalytic H₂ evolution on CdS by loading MoS₂ as cocatalyst under visible light irradiation. J. Am. Chem. Soc. 130, 7176–7177 (2008).
- 9. Hu, Y. et al. Carbon-coated CdS petalous nanostructures with enhanced photostability and photocatalytic activity. Angew. Chem., Int. Ed. 52, 5636–5239 (2013).
- Yang, J., Wang, D., Han, H. & Li, C. Roles of cocatalysts in photocatalysis and photoelectrocatalysis. Acc. Chem. Res. 46, 1900–1909 (2013).
- 11. Tang, Z. R., Yin, X., Zhang, Y. H. & Xu, Y. J. Synthesis of titanate nanotube—CdS nanocomposites with rnhanced visible light photocatalytic activity. *Inorg. Chem.* **52**, 11758–11766 (2013).
- Xu, X. J. et al. Controlled growth from ZnS nanoparticles to ZnS-CdS nanoparticle hybrids with enhanced photoactivity. Adv. Funct. Mater. 25, 445-454 (2015).
- 13. Bera, R., Kundu, S. & Patra, A. 2D Hybrid nanostructure of reduced graphene oxide—CdS nanosheet for enhanced photocatalysis. *Appl. Mater. Interfaces* 7, 13251–13259 (2015).
- Guan, G. Q. et al. Photocatalytic activity of CdS nanoparticles incorporated in titanium silicate molecular sieves of ETS-4 and ETS-10. Appl. Catal. A: Gen. 295, 71–78 (2005).
- Li, W.J. et al. Microwave synthesis of Zn_xCd_{1-x}S nanorods and their photocatalytic activity under visible light. J. Phys. Chem. C 114 2154–2159 (2010).
- Lu, X. X. et al. Novel mesoporous Zn_xCd_{1-x}S nanoparticles as highly efficient photocatalysts. Appl. Catal. B: Environ. 125, 11–20 (2012).
- 17. Maeda, K. et al. Photocatalyst releasing hydrogen from water. Nature 440, 295-295 (2006).
- 18. Wang, D. F., Kako, T. & Ye, J. H. Efficient photocatalytic decomposition of acetaldehyde over a solid-solution perovskite (Ag_{0.75}Sr_{0.25}) (Nb_{0.75}Ti_{0.25})O₃ under visible-light irradiation. *J. Am. Chem. Soc.* **130**, 2724–2725 (2008).
- Li, W. J. et al. High-efficient degradation of dyes by Zn_xCd_{1-x}S solid solutions under visible light irradiation. J. Phys. Chem. C 112, 14943–14947 (2008).
- Wang, W. Z., Zhu, W. & Xu, H. L. Monodisperse, mesoporous Zn_xCd_{1-x}S nanoparticles as stable visible-light-driven photocatalysts. J. Phys. Chem. C 112, 16754–16758 (2008).
- 21. Zhong, X. H. et al. Synthesis of high-quality CdS, ZnS, and Zn_xCd_{1-x}S nanocrystals using metal salts and elemental sulfur. *J. Mater. Chem.* 14, 2790–2794 (2004).
- 22. Liu, W. H. et al. Compact cysteine-coated CdSe(ZnCdS) quantum dots for in vivo applications. J. Am. Chem. Soc. 129, 14530–14531 (2007).
- 23. Xu, X. et al. Fabrication and photocatalytic performance of a Zn_xCd_{1-x}S solid solution prepared by sulfuration of a single layered double hydroxide precursor. Appl. Catal. B: Environ. 102, 147–156 (2011).
- 24. Xi, Y., Cheung, T. L. Y. & Ng, D. H. L. Synthesis of ternary Zn_xCd_{1-x}S nanowires by thermal evaporation and the study of their photoluminesence. *Mater. Lett.* **62**, 128–132 (2008).
- 25. Wang, X. X. et al. Yellow-light generation and engineering in zinc-doped cadmium sulfide nanobelts with low-threshold two-photon excitation. *Nanotech.* 25, 325702 (2014).
- 26. Li, W. J. et al. Microwave synthesis of Zn_xCd_{1-x}S nanorods and their photocatalytic activity under visible light. J. Phys. Chem. C 114 2154–2159 (2010).
- 27. Liu, Y. K. et al. Wavelength-controlled lasing in $Zn_xCd_{1-x}S$ single-crystal nanoribbons. Adv. Mater. 17, 1372–1377 (2005).
- 28. Yin, J. Z. et al. Hierarchical ZnO Nanorod-Assembled Hollow Superstructures for Catalytic and Photoluminescence Applications. Cryst. Growth Design 10, 40–43 (2010).

Acknowledgements

This work is supported by the National Basic Research Program of China (Grant No. 2013CB922102 and 2011CB935800), the National Natural Science Foundation of China (Grant No. 51172106 and 21471076) and a Project Funded by the Priority Academic Program Development of Jiangsu Higher Education Institutions.

Author Contributions

Q.L. and F.G. guided the entire project, carried out data analyses and co-wrote the manuscript. Y.J. and H.Z. performed the experiments, XRD characterizations, and SEM investigations. L.W. performed TEM investigations. C.S. performed photocatalysis experiments. All the coauthors discussed the results and commented on the manuscript.

Additional Information

Supplementary information accompanies this paper at http://www.nature.com/srep

Competing financial interests: The authors declare no competing financial interests.

How to cite this article: Jin, Y. *et al.* Hollow $Zn_xCd_{1-x}S$ nanospheres with enhanced photocatalytic activity under visible light. *Sci. Rep.* **6**, 29997; doi: 10.1038/srep29997 (2016).

This work is licensed under a Creative Commons Attribution 4.0 International License. The images or other third party material in this article are included in the article's Creative Commons license, unless indicated otherwise in the credit line; if the material is not included under the Creative Commons license, users will need to obtain permission from the license holder to reproduce the material. To view a copy of this license, visit http://creativecommons.org/licenses/by/4.0/